Materials Chemistry and Physics 316 (2024) 129114

Contents lists available at ScienceDirect

Materials Chemistry and Physics

journal homepage: www.elsevier.com/locate/matchemphys

2D magnesium phosphate resorbable coating to enhance cell adhesion on titanium surfaces

Amir Elhadad [a], Mohamed A. Mezour [b], Lina Abu Nada [a], Samar Shurbaji [a], Alaa Mansour [c], Sophia Smith [b], Hanan Moussa [b], Lisa lee [d], Eva M. Pérez-Soriano [e], Monzur Murshed [b,f], Richard Chromik [d], Faleh Tamimi [g,*]

[a] Department of Pre-Clinical Oral Health Sciences, College of Dental Medicine, QU-Health, Qatar University, Qatar
[b] Faculty of Dentistry, McGill University, Montreal, Canada
[c] Sharjah University, United Arab Emirates
[d] Department of Mining and Materials Engineering, Montreal, Canada
[e] Escuela Politécnica Superior, Universidad de Sevilla, Seville, Spain
[f] Division of Experimental Medicine, Department of Medicine, McGill University, Canada
[g] College of Dental Medicine, QU-Health, Qatar University, Qatar

HIGHLIGHTS

- 2D magnesium phosphate hydrogels can be used to produce stable coatings on Titanium surfaces.
- 2D magnesium phosphate coatings are biodegradable.
- 2D magnesium phosphate coatings enhanced protein adsorption as well as osteoblast adhesion and proliferation.
- The properties 2D magnesium phosphate coatings on titanium can be improved by thermal and chemical pre-treatment of Titanium.

GRAPHICAL ABSTRACT

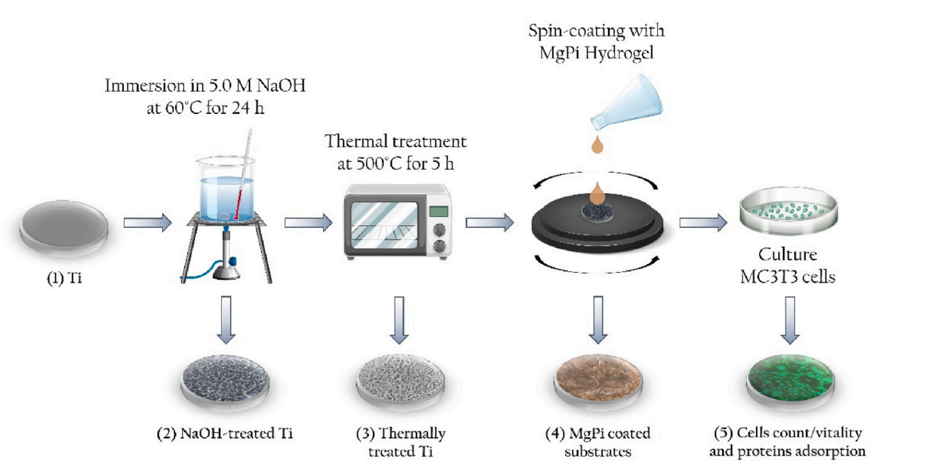

ARTICLE INFO

Keywords:
Titanium
Bioactivity

ABSTRACT

Titanium and its alloys are essential metals for orthopedic implant manufacturing due to their exceptional mechanical properties and biocompatibility, used extensively for treating various orthopedic conditions. However, Titanium (Ti) implants have a disadvantage due to lack of bioactivity, potentially affecting osseointegration

* Corresponding author.
E-mail addresses: aelhadad@qu.edu.qa (A. Elhadad), mohamed.mezour@mail.mcgill.ca (M.A. Mezour), lina.abunada@QU.EDU.QA (L. Abu Nada), Ss1104427@qu.edu.qa (S. Shurbaji), alaa.mansour@mail.mcgill.ca (A. Mansour), sophia.smith@mail.mcgill.ca (S. Smith), hanan.moussa@mail.mcgill.ca (H. Moussa), lisa.lee@mail.mcgill.ca (L. lee), evamps@us.es (E.M. Pérez-Soriano), Monzur.murshed@mcgill.ca (M. Murshed), richard.chromik@mcgill.ca (R. Chromik), fmarino@qu.edu.qa (F. Tamimi).

https://doi.org/10.1016/j.matchemphys.2024.129114
Received 22 November 2023; Received in revised form 16 February 2024; Accepted 20 February 2024
Available online 27 February 2024

Magnesium phosphate
Coatings
Protein adsorption

and osteoconductive capabilities, and may take several months to integrate with bone tissue. In this work, we prepared a layer of 2D magnesium phosphate (MgPi) coating on the surface of titanium surfaces *via* the spin-coating technique. Various techniques were used to study the phase composition of the coatings, including FTIR, Raman spectroscopy, NMR, and XRD analysis. Morphology and chemical analysis were performed using Atomic force microscopy and SEM/EDX. Nano-scratch test and water contact angle measurements were used to measure adhesion strength and wettability. In addition, in vitro cell assays were used to assess cell adhesion and viability to determine how the MC3T3-E1 osteoblast-like cells reacted to the different treated Ti substrates. AFM results showed that the surface roughness became lower after coatings. MgPi-coated samples showed higher hydrophilicity, protein adsorption, and cell viability than uncoated samples. The nano-scratch test showed that the MgPi coating showed better adherence to chemically and thermally treated samples compared to untreated samples. The deposited MgPi coating has good adhesion to the Ti-substrates. Most significantly, compared to uncoated control (Ti) ($p < 0.005$) and chemically treated coated samples CT-MgPi ($p < 0.005$), MC3T3-E1 cell proliferation was significantly increased on thermochemical coated surfaces. These findings point to resorbable two-dimensional MgPi coatings as a potential candidate for promoting Ti implant osseointegration.

Statement of significance

Despite pure titanium and its alloys being the most popular materials for long-term use as orthopedic implants, poor osseointegration is one of its drawbacks. We demonstrated that coating Ti-substrates with 2D magnesium phosphate (MgPi) enhanced cell response, including adhesion and cell viability, ultimately favorable for tissue repair and bone regeneration.

1. Introduction

Owing to their excellent corrosion resistance, biocompatibility, machinability, and load-bearing capacity, titanium (Ti) and its alloys are extensively employed in orthopedic implants [1,2]. However, due to the inert native surface oxide layer that typically forms on the surface of Ti-based implants, their poor and prolonged osseointegration continues to be a significant clinical challenge[3,4]. To improve osseointegration and promote the local bioactivity of Ti implants, a variety of strategies for surface modification using physical, chemical, and biochemical treatment approaches have been developed in recent years [5,6]. There are several methods for modifying the surface of titanium to improve osseointegration [3,7,8]. Some of the proposed techniques include etching and coating with a bioactive layer [9]. Etching is often regarded as the gold standard for osseointegration enhancement, yet it produces rougher surfaces [9,10]. Earlier research has shown that surface roughness enhances osteoblast attachment, proliferation, and differentiation, accelerating bone repair [4,11]. One possible way to improve early osseointegration is to employ a resorbable coating that could stimulate bone formation during the early stages of implant placement and then resorb. Hydroxyapatite HAp has been employed extensively for bone tissue engineering [12,13]. However, due to cracking, delamination, and HAp decomposition at the interface between the implant and the bone tissue, these coatings have had limited clinical success [14,15]. In addition, Furthermore, in vivo, tests have revealed that the synthetic crystalline HAp is not bioresorbable [16,17]. In contrast, Magnesium (Mg) alloys or Mg-coatings on metal substrates have recently been introduced for medical applications [18]. Magnesium is an essential element involved in many physiological functions [19,20]. Additionally, it is the fourth-most abundant cation in living organisms and the second-most abundant cation in cells [21,22]. Magnesium-based biomaterials are considered biocompatible and biodegradable and hold great potential for use in biomedicine [11,23]. Due to the presence of both magnesium and phosphorus in the human body, magnesium phosphates have become increasingly popular in biomedical sectors in recent years [11]. Mg and phosphorus are both abundant elements in the human body, and MgPi biominerals such as struvite ($MgNH_4PO_4.6H_2O$), newberyite ($MgHPO_4.3H_2O$), and cattiite ($Mg3(PO_4)_2.22H_2O$) naturally occur in physiological and pathological mineralized tissues [24]. This helps explain the high biocompatibility of magnesium phosphate materials. Magnesium phosphates are employed in tissue engineering as coatings, cements, ceramics, scaffolds, and monodisperse particles in nanomedicine [25]. As a result, an Mg-based material might be employed as a resorbable coating on a titanium implant to improve early osseointegration. Our recent research revealed how the resorbable 2D MgPi nanosheets promoted collagen synthesis, osteoblast differentiation, and osteoclast proliferation, which sped up bone repair and osseointegration [26]. As a consequence, we hypothesized that a resorbable coating of 2D MgPi, successfully applied to alkaline-treated and thermally treated Ti surfaces using a simple and cost-effective spin-coating technique, is a successful way to improve the surface biocompatibility of Ti implants, promoting osseointegration.

This work presents a novel approach for enhancing the biological properties of Ti surfaces using 2D magnesium phosphate hydrogel coatings. Here we describe the coating process and characterize their in vitro biodegradation, surface proteomics, and cytocompatibility.

2. Materials and methods

2.1. Titanium substrates

Commercially pure titanium (Cp-Ti, grade 5, McMaster Carr), ($n = 48$), with a diameter of 0.9 cm and a thickness of 0.5 mm, was abraded using progressively finer silicon carbide abrasives, 320, 600, 1200, and 2000. It was then ultrasonically cleaned for 20 min each in dd-H_2O, acetone, and EtOH before being dried for 12 h at 40 °C in an oven.

2.2. Pretreatment of Ti-substrates

The Cp-Ti, Ti-substrates ($n = 16$) were dried at 40 °C for 24 h before being immersed in 100 ml of 5.0 M NaOH solution for 24 h at 60 °C. The samples were then gently washed with dd-H_2O to remove the loosely bound Na^+ ions. Throughout the course of our current study, the samples treated with NaOH ($n = 16$) are referred to as chemically treated (CT). The term "thermo-chemically treated samples" (CTT) refers to half of these samples ($n = 8$) Ti-substrates that underwent further thermal treatment at 500 °C for 5 h in an air environment at a heating rate of 5 °C/min.

2.3. Hydrogel preparation

2D Magnesium phosphate hydrogel was prepared by adding a solution of 1.5 M phosphoric acid (H_3PO_4, sigma Aldrich) to 0.09 g magnesium hydroxide ($Mg\ (OH)_2$, Fisher, Belgium) while continuously stirring the solutions at room temperature. Then, a 1.5 M sodium hydroxide solution (NaOH, Fisher, Belgium) was added. Magnesium phosphates hydrogel was obtained when the mixture was hand-shacked for 20 s and allowed to age overnight.

2.4. Coating using spin-coater

A WS-400 Spin Coater (Laurell Technologies Corporation, USA) set to 3000 rpm for 30 s was used to deposit 250 μL of magnesium phosphate hydrogel on the Ti-substrates. The Ti-substrates were then left to dry for 24 h at room temperature. Schematic Diagram 1 depicts the various modifications to the Ti-substrates.

2.5. Characterization

Attenuated total reflectance infrared spectroscopy (ATR-IR) measurements were carried out on the coated and uncoated Ti-substrates using a Bruker Tensor 27 IR spectrometer (Bruker Optics Ltd., Coventry, UK) fitted with a deuterated triglycine sulfate pyroelectric detector with an accumulation of 16 scans in the 400–4000 cm^{-1} range at a resolution of 4 cm^{-1}. Additionally, Raman spectra were acquired using a SENTERRA-BRUKER German spectrometer in the range of 100–1000 cm^{-1} with a wavelength of 780 nm that had been excited from a Helium-Neon (HeNe) laser. Grazing Angle X-ray diffraction (GAXRD) was carried out for structural identification of coated and uncoated Ti-substrates. XRD patterns are recorded with (AXS GmbH diffractometer, Bruker, Germany), using a Cu K_α radiation source ($\lambda K_\alpha =$ 1.5406 Å), generated at 40 kV and 40 mA, grazing incidence at 3° within the 2θ range 10–60°.

The chemical composition and the binding state of elements in the MgPi coated and uncoated Ti-substrates were characterized by X-ray photoelectron spectroscopy (Thermo Scientific K_α spectrometer) using the Mg K_a X-ray source and pass energy of 50 eV. All the spectra were calibrated at the C1s binding energy (284.8 eV). The survey spectra in the range of 0–1100 eV were recorded in 1 eV step for each sample, followed by high-resolution spectra over different element peaks in 0.1 eV steps. To prevent surface charging, samples were hit with a flood gun shooting. The Thermo Avantage software (version 5.96) was used to carry out the peak-fitting processes. In order to explore the 2D nature of the material, microscopy images of the hydrogels were aquired using cryo-TEM. Five microliters of the hydrogel were applied to a glow-discharged holey carbon grid (C-Flat R2/2, Protochips, Inc), blotted, and frozen in liquid ethane using the Vitrobot Mark IV (Thermo Fischer Scientific, Hillsboro, OR, USA). High magnification micrographs of the sample were then captured using a Titan Krios 300 kV Cryo-S/TEM equipped with a Falcon 2 direct electron detector (DED and phase plate (Thermo Fischer Scientific, Hillsboro, OR, USA).

An Inspect-50 field emission scanning electron microscopy (SEM) (FEI, Japan) operating at 10 kV voltage was used to assess the morphology of the coated and untreated Ti-substrates. Atomic force microscopy (AFM) was used to investigate the changes in surface roughness induced by different treatments or MgPi coating of the Ti-substrates. The surface roughness measurement was performed at ambient conditions using an AFM instrument: a Nanoscope Multimode 8 equipped with a Nanoscope V controller (Bruker, Santa Barbara, CA). The topographies were acquired in peak force mode (Bruker ScanAsyst mode and Nanoscope 8.15r3 software). In peak force mode, silicon nitride cantilevers (ScanAsyst-Air Bruker) with a nominal spring constant of 0.4 N/m, a nominal resonance frequency of 50–90 kHz, and a nominal tip radius of 2 nm were used for imaging in air. AFM image analysis was performed using WSxM, 69 Nanoscope Analysis1.4, and IAPro-3.2.1 software.

2.6. Coating adhesion

Nano-scratch tests with a nanoindenter (Ubi3, Hysitron, US) were used to evaluate the adhesion strength between the coating and the Ti-substrates. A stylus with a diamond conical tip with a 2 μm radius was used for scratch testing. A ramp load from 0 to 10 μN was applied over 10 μm at a scratch rate of 0.66 μm/s. Five measurements were performed at room temperature for each sample. The average value of the critical load and the lateral force at the critical load of coated samples were compared.

2.7. Wettability, in vitro degradation, and protein adsorption of the coating

The wettability of the MgPi-coated and uncoated Ti surfaces was assessed by measuring the contact angle of 2 μL drops of distilled water (polar fluid) on the surface of the samples. The sessile drop method was used for contact angle measurements using a Video-based Optical Contact Angle Measuring Instrument (OCA-15 Plus) controlled by a SCA20 software module from Data Physics supplied by Neurtek SA (Spain). Three drops per sample were analyzed to calculate a mean and standard deviation. To assess the in-vitro degradation of the MgPi coatings, the coated Ti–substrates were immersed in 50 ml of rat plasma (Innovative Research, MI, USA) that had been diluted to a concentration of 1% using phosphate buffer solution (PBS). After being immersed in separate plastic containers, the samples were incubated at 37 °C. One ml of the diluted rat plasma was collected from each container After 1, 3, 5, and 7 days and stored frozen until being analyzed using inductively coupled plasma (ICP) (Thermo Scientific iCAP 6500 dual view, UK). The changes in surface morphologies of MgPi coatings after immersion in diluted rat plasma were also investigated using SEM.

While immersed in plasma proteins, coated and uncoated Ti-substrates were examined for their affinity to protein adsorption. For the protein adsorption test, equal volumes of rat plasma (Innovative Research, MI, USA) diluted with PBS to 1% at 37 °C were incubated with a set of coated and uncoated Ti-substrates for 3 h at room temperature. The samples were then rinsed with PBS to remove any proteins that were only marginally adhering. The incubated samples were then subjected to a mass spectrometry analysis. The database search results were loaded onto Scaffold Q + Scaffold_4.4.8 (Proteome Software Inc., Portland, Oregon, USA) for spectral counting, statistical treatment, and data visualization.

2.8. In-vitro cellular proliferation

To aid in the adhesion of the cells, MC3T3 cells were cultured using the ring culture technique on top of MgPi-coated and uncoated Ti-substrates. Briefly, plastic cylinders of constant diameter (5 mm) were attached to the substrate surface. The substrates were sterilized, and polystyrene cloning cylinders (Sigma) were attached to the disks using vacuum grease. MC3T3-E1 cells from ATCC (Manassas, VA, USA) were cultured in alpha-MEM (Invitrogen, Carlsbad, CA, USA). Culture media were supplemented with 10% FBS (PAA, Etobocoke, Ontario, Canada) and 100 U/ml penicillin-streptomycin (Invitrogen, Carlsbad, CA, USA). Cells were grown at 37 °C under 5% CO_2 in a humidified incubator. MC3T3 cells were cultured on top of Ti-substrates treated with six different conditions (Ti, CT, CTT, Ti-MgPi, CT-MgPi, CTT-MgPi) as described in Fig. 1. The medium was changed every two days. Cells were stained with calcein (Sigma-Aldrich, Saint Louis, MO, USA) and incubated for 20 min inside the incubator; after that, cells were washed three times and were fixed with 4% paraformaldehyde and incubated for 5 min at room temperature. After washing three times in PBS, H33258 nuclear staining was performed, and then washed once in PBS. Cells grown on Ti-substrates' surface were imaged using an inverted fluorescent microscope (EVOS FL, Thermo Fisher Scientific), and cell nuclei were counted. Five titanium disks were analyzed per group, and three regions of interest were selected randomly on each disk.

2.9. Statistical analysis

The data were evaluated for normal distribution using the Shapiro-Wilk test. For data following normal distribution, one-way ANOVA with post-hoc using Tukey HSD test was done, and pairwise comparison was then applied to detect significant differences among groups. The

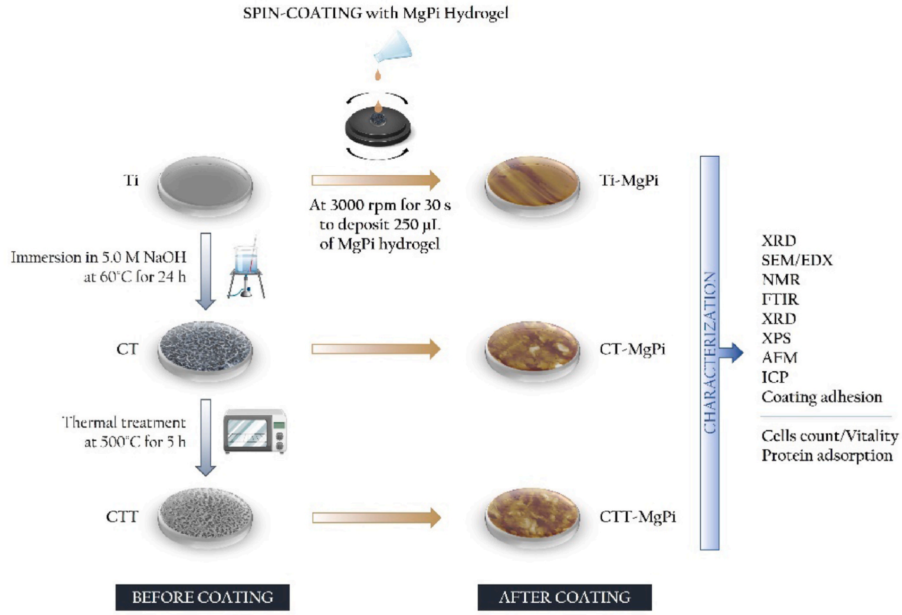

Fig. 1. Schematic illustrations of the modifications made on Ti-substrates: (Ti) untreated; (CT) immersed in 5.0 M NaOH at 60 °C for 24 h; (CTT) immersed in 5.0 M NaOH at 60 °C for 24 h followed by thermal treatment at 500 °C for 5 h; (Ti-MgPi) bare Ti-substrate coated with MgPi hydrogel; (CT-MgPi) CT-substrate coated with MgPi hydrogel; and (CTT-MgPi) CTT-substrate coated with MgPi hydrogel.

statistical significance level was set at $p < 0.05$. IBM_ SPSS_ (v. 17, IBM Corp.; New York; USA) software was used for data analysis, and graphs were generated using GraphPad Prism version 6.01). Scaffold_4.4.8 software was used to analyze the proteomic data using Fisher's exact test to assist protein adsorption to Ti-substrates.

3. Results and discussion

Immediately upon preparation at room temperature (25 °C), the prepared MgPi was in the sol state (Fig. 2a the vials were flipped upside down after the overnight incubation to examine the flow. The hydrogel formulation showed thixotropic shear-thickening behavior and could maintain a gel state. According to the SEM micrographs used for morphology analysis, the dried MgPi powder had irregular 2D crystals (Fig. 2b and c). Fig. 2d and e show two representative environmental-TEM micrographs of a 1% v/v magnesium phosphate colloid dispersion in water. The TEM micrographs reveal the very thin 2D nanosheet structure of the material. A schematic diagram of the proposed structure of the MgPi hydrogel (Na_3PO_4+/$MgHPO_4^-$/Na_3PO_4 $^+$) is shown in Fig. 2f. According to FTIR, XRD, and NMR studies, the structure of the MgPi is mainly composed of polyhedrons of PO_4^{3-} (Fig. 2 g-i). Results in the literature indicated that rough implant surfaces as well as coated implant surfaces could increase osseointegration [27,28].

The ATR-IR spectra of the coated and untreated Ti-substrates are shown in Fig. 2j. All spectra displayed tiny bands related to stretching Ti-O and Ti-O-Ti vibrations between 650 and 800 cm^{-1}, with notable TiO_2 lattice vibrations at around 794 cm^{-1} [3,7,29]. The relatively small band at 831 cm^{-1} corresponds to the Ti–O–Ti asymmetric stretch, belonging to oxygen-bridged titanium (IV) oxides [7]. The formation of a Na-titanate hydrogel layer on the Ti –substrates as a result of NaOH treatment is verified by the band at 1353 cm^{-1} in the spectrum of the CT substrate, which may be attributed to different types of Na-titanate compounds [30]. In the spectra of coated Ti-substrates (Ti-MgPi, CT-MgPi, and CTT-MgPi), two distinct bands are observed in the range of 997–1060 cm^{-1}, which are attributable to symmetric (ν_1) and anti-symmetric (ν_3) stretching vibrations of the P-O bond in PO_4^{3-} at 997 and 1060 cm^{-1}, respectively [31,32]. These bands indicate the reordering of the polyhedrons of PO_4^{3-} in the structure of the deposited MgPi layer. Raman spectroscopy measurements were used to support the ATR-IR findings. The Raman spectra of Ti-substrates discs with and without MgPi coating are displayed in Fig. 2k. The passive oxide layer that generally forms on the surface of titanium is amorphous. Hence, no crystalline peaks were observed in the spectra of the untreated sample (Ti) [33]. The spectrum of the NaOH-treated Ti-substrates (CT) shows a set of four peaks. The peak at 440 cm^{-1} is assigned to Ti-O bending vibration involving three-fold oxygen; Peaks at 682 and 806 cm^{-1} are attributed to Ti-O bending and stretching vibrations involving twofold oxygen, while a peak at 901 cm^{-1} is attributed to Ti-stretching vibration involving non-bridging oxygen, some of which are coordinated with Na^+ ions [34]. These peaks show that the reaction with NaOH solution on the surface of the chemically treated Ti-substrates resulted in the formation of sodium hydrogen titanate (SHT), $Na_xH_{2-x}Ti_3O_7$. These findings align with previous studies on hydrogen titanate (HT). The Raman spectra of the MgPi coated Ti-substrates, (Ti-MgPi, CT-MgPi, and CTT-MgPi) revealed a band attributed to the PO_4^{3-} group's stretching mode produced at 967 cm^{-1} [8,35]. These results clearly demonstrated that MgPi has been successfully deposited on both untreated and treated Ti-substrates.

Grazing angle X-ray diffraction (GAXRD) was used to examine the Ti-substrate's phase assemblage. The GAXRD data of MgPi coated and uncoated Ti-substrates are summarized in Fig. 2l. The bare (Ti) sample's spectrum shows Ti peaks at 2θ 38.95, 35.02, 40.66, and 53.70° [36]. Additionally, for the (CT) sample, tiny peaks of the sodium hydrogen titanate phase (SHT) were seen at 2θ 49.25, 31.43, and 28.69° [37]. These peaks result from the NaOH-treated surface porous network layer [37]. The sodium titanate (ST) phase was observed at 2θ 249.71° in the diffractogram of the thermo-chemically treated sample (CTT) [38]. This indicates that during thermal treatment, the (SHT) phase transforms into the (ST) phase [39].

Following coating deposition, the prominent crystalline peak's intensity at 2θ 38.95, 35.02, 40.66, and 53.70° decreased for the coated samples, which include (Ti-MgPi), (CT-MgPi), and (CTT-MgPi) samples. This is due to the crystalline structure of the deposited MgPi layer, which masked the phases from the Ti-substrates beneath.

The XPS survey spectra of the MgPi-coated and uncoated Ti-substrates are shown in Fig. 3a. The survey spectra show the presence

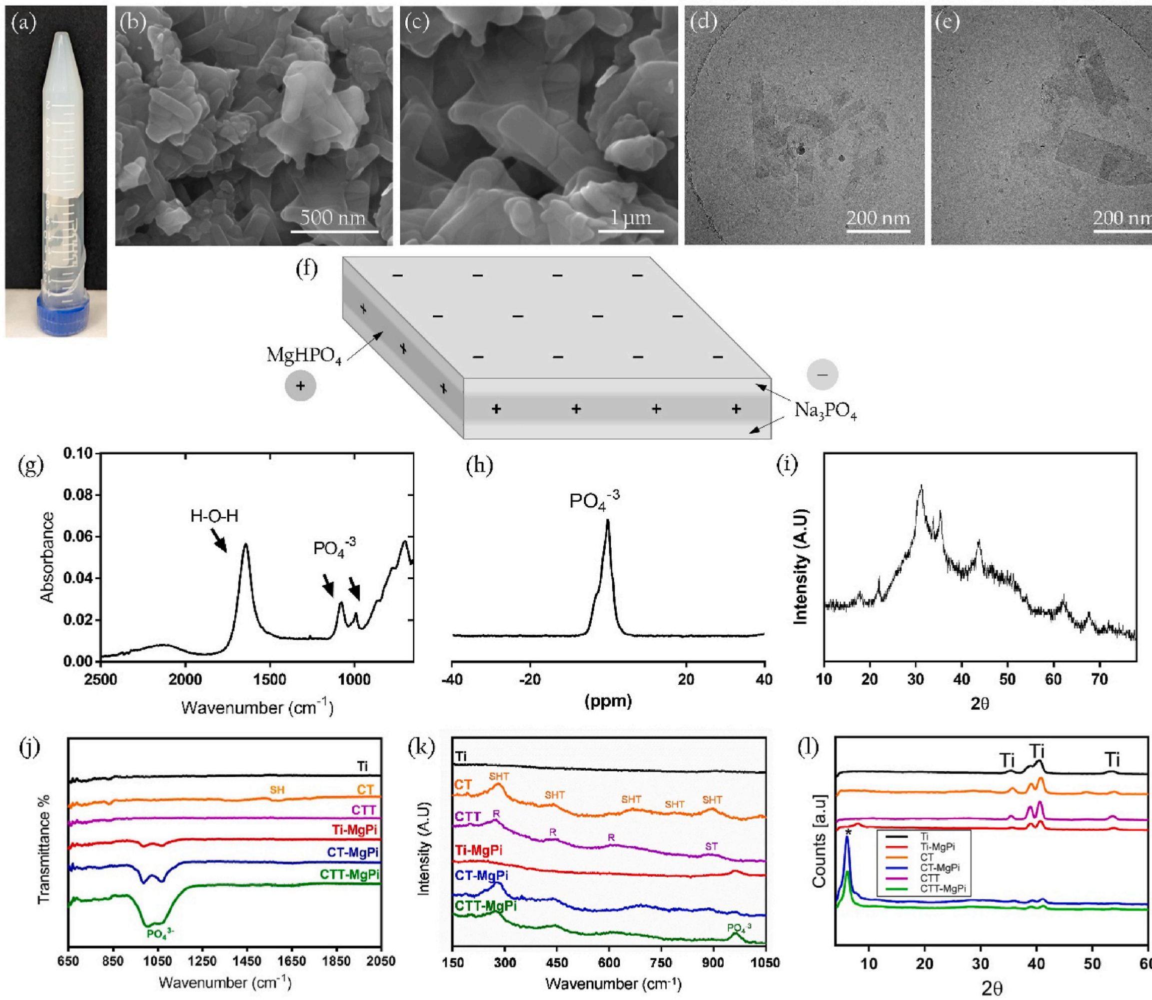

Fig. 2. (a) Thixotropic MgPi hydrogel; (b and c) SEM micrographs of the dried MgPi hydrogel; (d and e) Environmental-TEM micrograph of a MgPi colloidal dispersion with a concentration of 1% v/v in water; (f) 2D structure of the MgPi hydrogel; (g) FTIR spectrum of the dried MgPi hydrogel; (h) NMR spectrum of the dried MgPi hydrogel; (i) XRD pattern of the dried MgPi hydrogel; (j) ATR-IR; (k) Raman spectra; (l) GA-XRD patterns for MgPi coated and uncoated Ti-substrates (Ti: titanium, R: rutile, SHT: sodium hydrogen titanate, ST: sodium titanate).

of Ti, O, and C signals in the bare sample (Ti), whereas Ti, O, C, and Na are seen in Ti-substrates that have been chemically or thermo-chemically treated, ((CT) and (CTT)). Signals for Ti, O, C, Na, P, and Mg have been seen in coated samples (Ti-MgPi), (CT-MgPi), and (CTT-MgPi). The C peak's appearance indicated surface contamination from exposure to air prior to the XPS measurement. Table 1 lists the relative chemical composition of the prepared samples. The only prominent signals for uncoated Ti-substrates (Ti) are Ti, O, and C. Ti2p′s photoelectron peak is clearly visible at a binding energy of 459.08 eV, O1s at a binding energy of 531.08 eV, and C1s at a binding energy of 284.8 eV [40]. Ti, O, C, and Na signals are observed after NaOH and thermo-chemical treatment, including both (CT) and (CTT) samples. This indicates that the formed layer is sodium hydrogen titanate. It has been established that the concentration of Na increases in the NaOH-treated samples compared to the untreated (Ti) samples and that Na is also detected as a peak at 1070.98 eV after NaOH treatment [41]. This peak's appearance and the broadening and intensification of the Ti-O peak at 530.4 eV suggest that Ti surface has developed a sodium titanate layer as a result of NaOH treatment [40]. The XPS of O1s core levels of the coated and uncoated Ti-substrates with MgPi (Fig. 3b) are broad in nature and could possibly be curve-fitted into several component peaks. Following deconvolution, the binding energy peaks at 529.6 and 531.5 eV are attributed to a combination of the oxygen from the titanium dioxide (Ti–O bond of TiO_2), titanium hydroxide (hydroxyl groups of Ti–hydroxide (Ti–OH)), respectively [42].

The compound with the binding energy peak of 535.2 eV corresponds to H_2O, which originated from the physically adsorbed H_2O [43]. The thin passive layer of titanium oxide on the surface of the untreated bare (Ti) sample caused it to produce an O1s peak at 529.6 eV [42]. However, the sodium titanate and rutile that were produced on the surfaces of the NaOH and NaOH-thermally treated Ti-substrates (CT) and (CTT) samples, respectively, produce a clear O1s peak to be attributed to the Ti-O bond in these samples.

The Ti-OH group's atomic concentration rises from 24.3% in the untreated Ti sample to 34.6% in the NaOH-treated CT sample. The chemical reaction between Ti and NaOH could be responsible for this increase (Table 2). The Ti2p spectrum (Fig. 3d), which is a doublet with Ti2p3/2 and Ti2p1/2 at 458.2 and 463.9 eV, respectively, is shown by the high-resolution Ti2p of the (Ti), indicating the presence of Ti^{3+} (Ti-O) [44].

The Ti-O signal at 530.5 eV in the high-resolution O1s spectrum, as shown in (Fig. 3b), confirms the existence of this surface oxide layer. Peaks from Ti^{2+} (Ti-O) are attributed to a second doublet with Ti2p3/2 and Ti2p1/2 at 463.98 and 455.48 eV, respectively. Assigned to peaks from metallic Ti, a third doublet seen at 453.48 eV (Ti2p3/2) and 459.38 eV (Ti2p1/2) shows that Ti-Ti bonding is only seen on the uncoated Ti substrates [44]. The remaining dominating peaks have been detected as Ti^{4+} (Ti-O) 2p3/2 at 458.3 eV and Ti^{4+} (Ti-O) 2p1/2 at

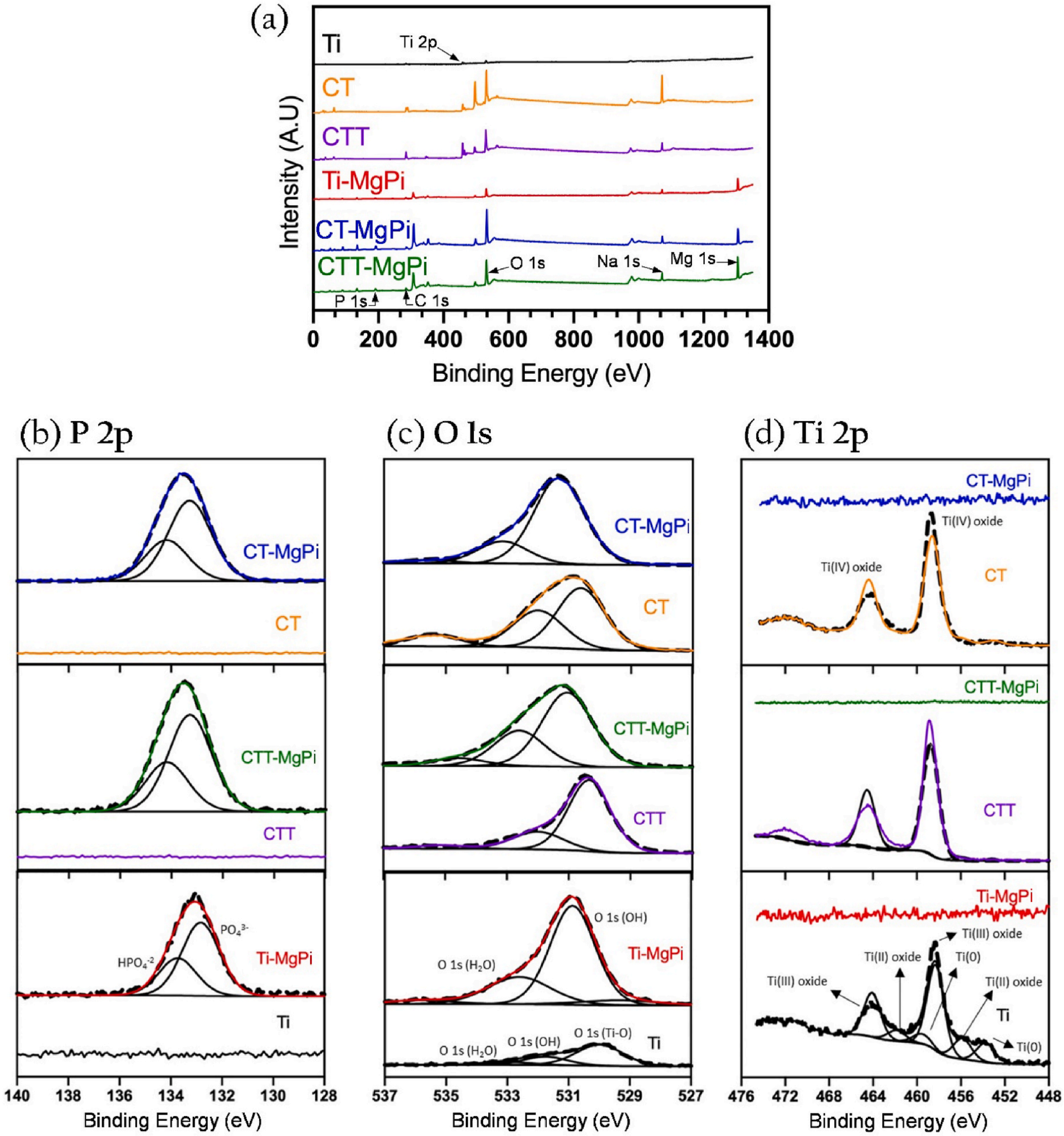

Fig. 3. (a) XPS survey spectra of 2D nanocrystalline MgPi coated and uncoated Ti-substrates; (b, c, and d) Curve-fitted P2p, O1s, and Ti2p for the MgPi coated and uncoated Ti-substrates.

Table 1
Surface Atomic concentration percentage of the MgPi coated and uncoated Ti-substrates obtained by the XPS.

Samples	Atomic concentration (%)					
	Ti	O	C	Na	Mg	P
Ti	15.5 ± 0.2	47.8	36.6 ± 0.2	–	–	–
CT	4.9 ± 0.4	49.6 ± 1.67	28.5 ± 2.2	16.8 ± 0.95	–	–
CTT	20.9 ± 0.3	54.5 ± 0.50	12.4 ± 0.9	12.0 ± 0.35	–	–
Ti-MgPi	–	55.8 ± 0.55	13.8 ± 0.7	7.5 ± 0.54	11.6 ± 0.8	11.±0.7
CT-MgPi	–	58.6 ± 0.49	10.4 ± 1.0	5.3 ± 0.47	12.5 ± 1.0	12.9 ± 0.2
CTT-MgPi	–	54.8 ± 3.60	12.7 ± 0.2	6.0 ± 0.83	14.8 ± 4.7	11.3 ± 1.3

464.6 eV after NaOH or NaOH-thermal treatment (CT) and (CTT) Ti-substrates. This is consistent with the findings of Raman, GAXRD, and ATR-IR, which revealed the presence of sodium titanate and rutile as the major phases on the surface (CT) and (CTT) samples.

Following the MgPi coating's deposition, the coated samples showed noticeable variations. Despite the presence of Na1s, Mg1s, P2p, O1s, and C1s, the continuous nature of the deposited layer is demonstrated by the absence of titanium peaks from the underlying Ti-substrates [45]. The peaks from the sodium MgPi layer's deposition, Na1s (1071.88 eV), Mg1s (1304.58 eV), and P2p (133.3 eV), are seen in each spectrum. $MgHPO_4$ from the deposited layer corresponds to the position of the Mg1s peak [46]. High-resolution XPS spectra of P2p confirmed the presence of two distinct phosphate anions, and its deconvolution into two peaks at 133.5 and 134.4 eV was assigned to PO_4^{3-} and HPO_4^{2-}, respectively [47], both of which could be recognized as the signal from MgPi coating.

Table 2
Atomic concentration percentage of the TiO_2, Ti–OH, H_2O peaks obtained by deconvoluting the XPS O1s spectra of the MgPi coated and uncoated Ti-substrates.

Samples	Atomic concentration % of the deconvoluted peaks				
	TiO_2	Ti-OH	H_2O	P-O	P-OH
Ti	88.08 ± 1.08	24.37 ± 0.19	9.55 ± 0.31	–	–
CT	54.06 ± 0.81	34.64 ± 1.1	11.31 ± 0.85	–	–
CTT	73.55 ± 1.27	22.08 ± 0.7	4.36 ± 0.14	–	–
Ti-MgPi	–	–	3.74 ± 0.12	69.41 ± 2.31	26.85 ± 0.33
CT-MgPi	–	–	3.12 ± 0.32	77.01 ± 1.55	19.87 ± 0.57
CTT-MgPi	–	–	6.74 ± 0.15	63.03 ± 1.38	30.22 ± 0.49

The SEM micrographs of the coated and uncoated Ti-substrates are shown in (Fig. 4a–f). According to micrographs, the bare titanium (Ti) sample surface is smooth with scratch patterns that form throughout the polishing process (Fig. 5a). After being subjected to NaOH treatment, the Ti-substrates surface developed a porous network structure with an interconnected pore network, as seen by the CT micrograph (Fig. 4b). According to EDX analysis, Na^+ ions were incorporated into the surface of the Ti metal after NaOH treatment. In comparison to those before the heat treatment, the Ti surface's porous network structure after thermal treatment with NaOH (CTT) is a little bit denser (CT) (Fig. 4c), with the Na signal remaining after heat treatment.

There is a noticeable difference between the microstructure of the coated and untreated Ti-substrates (Fig. 4 d-f). The mechanically polished scratches on the bare Ti-substrate disappeared, indicating that the coating was correctly applied. The uneven and rough surfaces of the MgPi-coated Ti-substrates (Ti-MgPi), (CT-MgPi), and (CTT-MgPi) were clearly visible. According to studies, coated and rough implant surfaces can encourage osseointegration [48]. The successful deposition of magnesium phosphate coating was verified by the EDX examination of the MgPi-coated surfaces, as evidenced by the presence of Mg, Na, and P signals (Fig. 4).

An in-depth analysis of the morphological differences was made possible by AFM's topographic characterization of the surfaces. The surface topographies of the uncoated Ti-substrates (Ti), NaOH-treated substrates (CT), and NaOH-thermally treated substrates (CTT) are shown (Fig. 4 a-c). The variations in surface roughness of these samples (Ti, CT, and CTT) were also assessed. The results of the AFM analysis show that the Ti surface that had been modified with NaOH (CT) had a surface that was significantly rougher (Ra = 53.95 ± 1.1 nm) than the untreated Ti substrate (Ra = 45.56 ± 1.42 nm) or the CTT sample that had undergone subsequent thermal treatment at 500 °C (Ra = 48.33 ± 1.09 nm). The coated Ti-substrates (Ti-MgPi), (CT-MgPi), and (CTT-

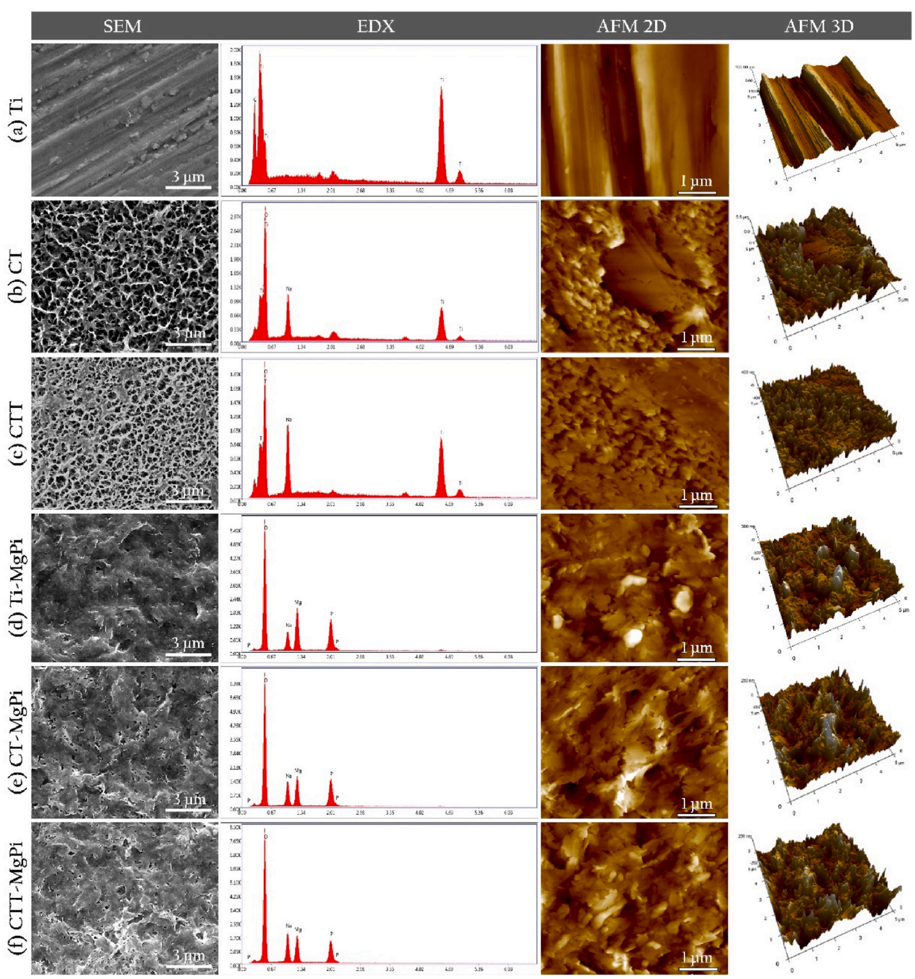

Fig. 4. SEM micrographs and corresponding 2D and 3D AFM micrographs of (a) Bare Ti; (b) Uncoated-CT substrate; (c) Uncoated-CTT substrate; (d) MgPi-coated Ti substrate; (e) MgPi-coated CT substrate; (f) MgPi-coated CTT substrate. In contrast to the more porous surface observed on the surface of NaOH-treated substrates (CT), the thermally treated Ti surface (CTT) is denser in the SEM micrographs of the uncoated substrates. The coated substrates' surface displayed irregular MgPi coatings.

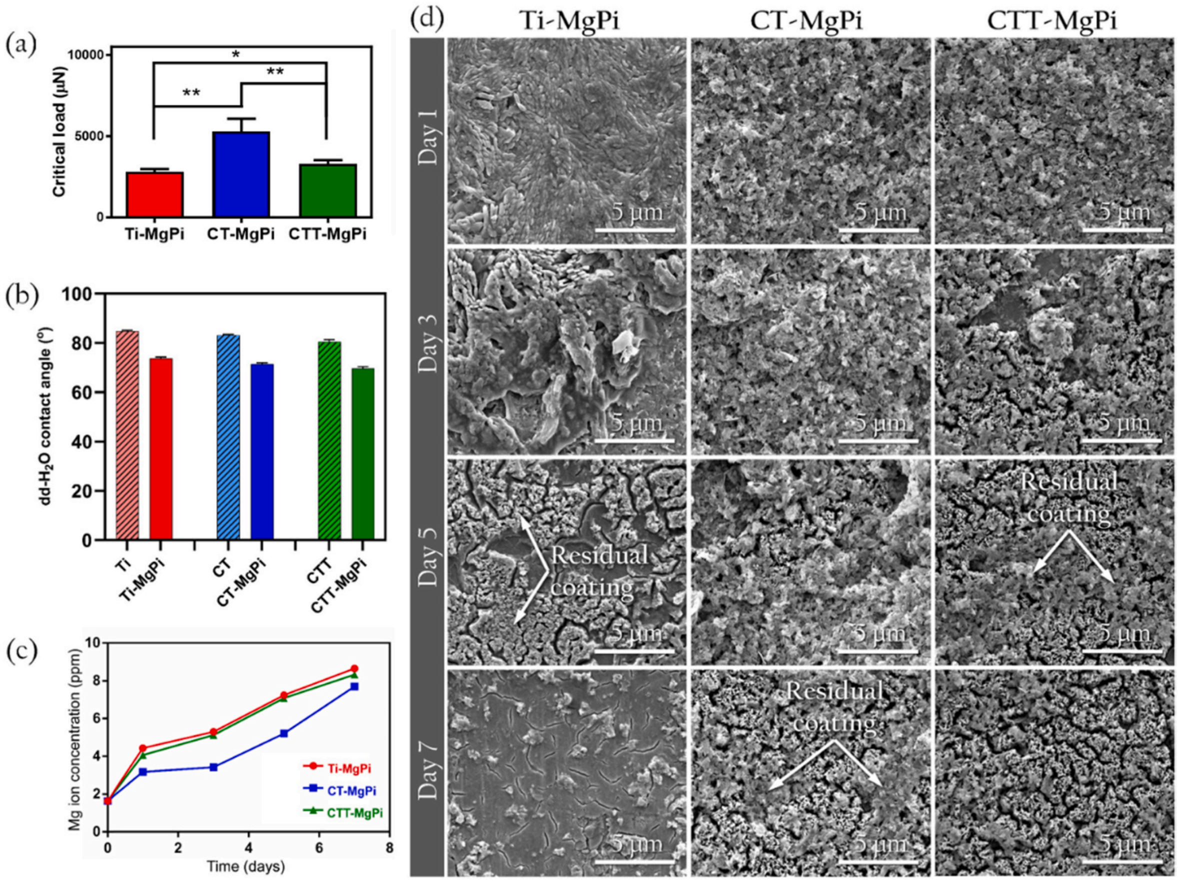

Fig. 5. (a) Bar graph comparing the critical load required to detach the MgPi coatings; (b) Water contact angle of MgPi coated and uncoated titanium surfaces; (c) Mg^{2+} concentration (ppm) released from Ti-MgPi, CT-MgPi, and CTT-MgPi coatings during biodegradation, in comparison to other groups, the MgPi coating on the chemically treated Ti substrate, (CT-MgPi) degrades more slowly; (d) High magnification (20000 ×) SEM images.

MgPi) had an average surface roughness of 36.20 ± 0.47, 37.45 ± 2.60, and 32.50 ± 0.44 nm, respectively. The R_a data show how the deposition of MgPi coatings changed the surface roughness and produced significantly smoother surfaces than uncoated substrates. Scratch patterns from the polishing process are the reason for the roughness of the uncoated sample. However, after coating deposition, the coating fills in these imperfections with a coating layer that covers them up, creating smoother coatings.

Scratch experiment was carried out on Ti-MgPi, CT-MgPi, and CTT-MgPi coatings using the same testing parameters to compare the coating adhesion to the Ti-substrates (Fig. 5 a). The average critical load was 5650 μN for Ti-MgPi coatings and 8270 μN for CTT-MgPi coatings. When a ramping load from 0 to 10 mN was applied, a critical load associated with coating detachment or fracture was not observed in the CT-MgPi coating, showing the critical load is higher than 10 μN. This indicates that the baseline Ti-coated sample (Ti-MgPi) has lower adhesion strength than the pre-treated coatings (CT-MgPi and CTT-MgPi). A better mechanical interlocking between the coating and the Ti substrate beneath may have been made possible by the improved surface roughness brought about by pre-treatments such as NaOH or NaOH-thermal treatments. This may have led to the improved adhesion of the pre-treated samples. The CT-MgPi coating offers superior scratch resistance than the other two coatings, as evidenced by the fact that its lateral force during scratch testing was consistently larger than that of the other two coatings, Ti-MgPi and CTT-MgPi.

A critical factor affecting cell adherence and protein adsorption is the wettability of metallic biomaterial surfaces. The contact angle (θ), which represents the angle where the liquid-gas and solid-liquid interfaces meet, indicates the degree of wetting [49]. The surface wettability of the resulting MgPi-coated and uncoated titanium surfaces was studied by measuring the contact angle of dd-H_2O using the sessile drop method. The mean contact angle and standard deviation for each surface are shown in Fig. 5b. For Ti, CT, and CTT uncoated surfaces, the prepared sample results show contact angles of 84.8 ± 0.39°, 83.16 ± 0.29°, and 80.5 ± 0.87°; for MgPi coated surfaces, the results show contact angles of 73.8 ± 0.5°, 71.43 ± 0.51°, and 69.7 ± 0.64° for Ti-MgPi, CT-MgPi, and CTT-MgPi coated samples. The MgPi-coated titanium samples exhibit a lower contact angle than the uncoated samples, suggesting that the MgPi-coated surfaces are more hydrophilic than the uncoated samples. The decrease in contact angle for titanium surfaces coated with magnesium phosphate coating might be attributed to the inorganic nature of the coating. Moreover, the MgPi-coated surfaces had contact angles ranging from 69.7 to 73.8°. An improvement in protein adsorption over the MgPi-coated samples should be expected, as the optimal contact angle range has been found to be between 60 and 80° [50].

In-vitro immersion studies were performed to evaluate the morphological changes brought on by the degradation of the MgPi coatings. The coated Ti-substrates (Ti-MgPi), (CT-MgPi), and (CTT-MgPi) are shown in SEM images at various times of immersion in rat plasma (Fig. 5d). All coated Ti-substrates exhibited deterioration and an increase in irregularities in surface morphology with time (Fig. 5d). All coatings completely degraded after seven days of immersion in plasma proteins, revealing the structure of the underlying Ti-substrates. During the immersion test, variations in the Mg^{2+} ion concentration were recorded using the inductively coupled plasma technique (ICP) (Fig. 5c). A rise in the concentration of Mg^{2+} was accompanied by a degradation of all coated Ti substrates, as seen in SEM micrographs. The CT-MgPi degraded more gradually than the Ti-MgPi and CTT-MgPi samples.

The degradation products of Mg^{2+} and PO_4^{3-} ions from MgPi coatings are easily discharged from the body through normal metabolism [25].

Preosteoblasts MC3T3-E1 cells were plated (3000 cells/disk) on each Ti-substrate for 4 days (Fig. 6). Following nuclear staining with H33258, the number of cells on coated Ti substrates (Ti-MgPi), (CT-MgPi), and (CTT-MgPi) was higher than on uncoated Ti-substrates Ti, CT, and CTT (Fig. 6). Additionally, MgPi coatings significantly ($p < 0.05$) increased cell proliferation as compared to uncoated titanium substrates (Ti), (CT), and (CTT) (Fig. 7d). The increase of calcein staining is used to measure cell viability. After four days of culture, MC3T3-E1 cells further showed an increase in cell proliferation on the coated samples (Ti-MgPi, CT-MgPi, and CTT-MgPi) in comparison to uncoated Ti-substrates (Ti, CT, CTT). On the contrary hand, thermal treatment (CTT) significantly increased cell proliferation compared to the untreated substrate (Ti) in the absence of MgPi coating ($p < 0.05$), (Fig. 7d). When the biological properties of the MgPi coatings were compared to in vitro cellular responses, it was found that they outperformed the Ti-substrates. While the initial cell attachment to the MgPi coatings showed that the cells proliferated more effectively and spread well, the cell proliferation and adhesion on both the MgPi coatings and treated Ti-substrates were favorable (Fig. 7d). The MgPi coatings' affinity for fibronectin adsorption and the changes in surface roughness across the coatings can be used to explain why 2D magnesium phosphate-coated Ti-substrates have better cell adhesion than uncoated Ti-substrates. These findings imply higher long-term functions of osteoblasts on MgPi-coated titanium, as both proliferation and adhesion of osteoblast are prerequisites for their deposition of bone [51].

The MgPi coatings' affinity for protein adsorption was evaluated using proteomics analysis after the bare (Ti) and coated (Ti-MgPi) samples were submerged in rat plasma for 3 h at 37 °C. (Fig. 7a–c). In accordance with our findings, more plasma proteins (97 proteins) were able to adsorb to the coated sample (Ti-MgPi) compared to the uncoated

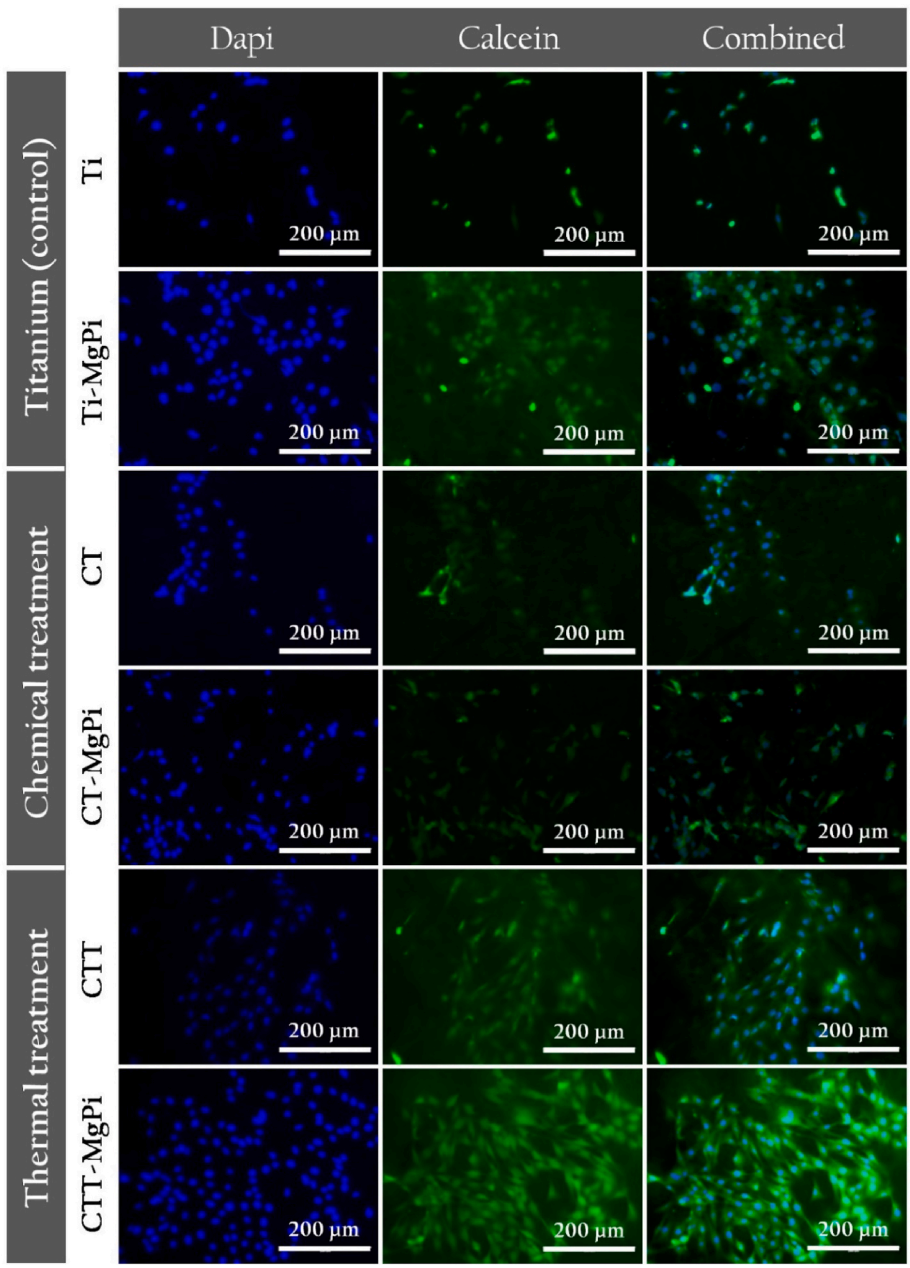

Fig. 6. Fluorescence microscopy showing stained MC3T3-E1 cells on the MgPi coated and uncoated Ti-substrates. The results showed more cells on the surface of the MgPi-coated Ti substrates than the uncoated substrates, indicating that MgPi coating has better biocompatibility without appreciable toxicity.

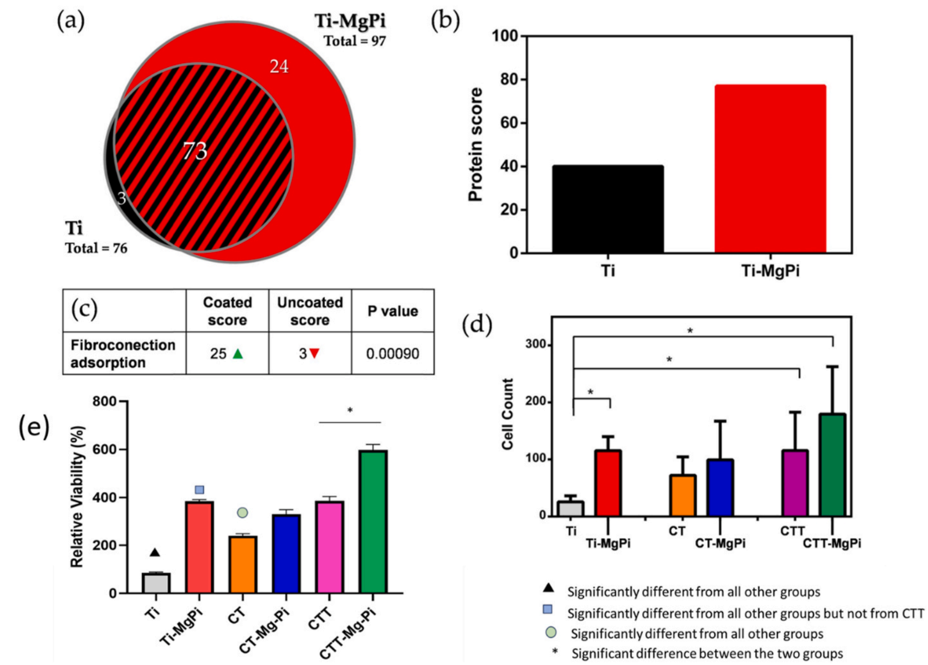

Fig. 7. (a,b) Proteomics mass spectrometry analysis, the coated sample (Ti-MgPi) showed higher plasma protein adsorption capacity (97 proteins) compared to the uncoated control (Ti) (76 proteins).(c) Table showing Mass spectrometry analysis result of the fibronectin adsorption; MgPi-Ti coated substrate showed a significantly higher fibronectin protein score compared to uncoated Ti substrate, Significance was found when $p < 0.05$. (d) Number of adhered cells on MgPi-coated and uncoated Ti substrates, The proliferation of MC3T3-E1 cells increased on coated samples (Ti-MgPi, CT-MgPi, and CTT-MgPi) after four days of culture in comparison to uncoated Ti-substrates (Ti, CT, CTT). (e) Cell viability of all experimental groups relative to the control cell culture well plate group.

control (Ti) (76 proteins). Furthermore, compared to their uncoated samples, coated samples showed a significantly higher fibronectin protein score, according to our findings. Fig. 7c displays the protein's scores in coated and uncoated Ti-substrates that were exposed to plasma proteins.

Cellular adhesion are mediated by the glycoprotein fibronectin, an important ingredient of the extracellular matrix (ECM), which interacts with integrin receptors on cell surfaces [52]. Fibronectin (FN) is believed to promote osteoblast and osteogenic cell responses in vitro, particularly cell adhesion, proliferation, differentiation, and survival [53]. Additionally, the accumulation of this protein is necessary for the migration, adhesion, and aggregation of numerous cell types during wound healing, including platelets, fibroblasts, and endothelial cells [54]. According to our study's findings, the coated surfaces showed greater protein adsorption affinity when compared to the uncoated surfaces.

The viability of all experimental groups was evaluated relative to a control group, defined as cells grown on a cell culture-treated dish (Fig. 7e). The control group's viability was set as the baseline at 100%. An observed viability percentage exceeding 100% indicates a proportional increase in the cell's viable cells compared to the control. The uncoated titanium sample (Ti) exhibited viability nearly equivalent to the control group, at (85.8%). However, the MgPi-coated titanium sample (MgPi-Ti) demonstrated a substantial increase, with a near quadrupling in cell number (384.76%). The uncoated thermally-treated titanium sample (CTT) also showed a similar increase, with viability of (385.5%). Remarkably, the thermal-coated titanium sample (CTT-MgPi) displayed a six-fold increase in viability (598%). The chemically treated titanium sample also showed significant improvement, with a two-fold increase (241%) in the uncoated condition (CT) and a three-fold increase (331%) when coated (CT-MgPi). Compared to untreated and uncoated titanium (Ti), the uncoated titanium surfaces that underwent chemical and thermal treatment (CT and CTT) had a higher cell count. This may be caused by the presence of Na on the surfaces due to the NaOH treatment. Cell adhesion has been seen to be positively impacted by alkali treatment, particularly when sodium is used [55]. As a consequence of this treatment, Na ions may enhance protein and cellular adhesion.

Conversely, as compared to uncoated surfaces, the MgPi-coated surfaces displayed a higher cell count. Since magnesium has been shown in several studies to promote bone formation, its presence in the coated discs can be directly related to boosting cell count and cell viability [56,57]. It has previously been established that animals with lower magnesium levels demonstrated osteoblastic growth and bone formation suppression. Similarly, a correlation between altered bone formation and Mg deficiency was reported in humans [58]. A lot of data has been reported suggesting the role of Mg in bone formation and remodeling.

4. Conclusion

This study shows that 2D magnesium phosphate can be used to produce mechanically stable, bioresorbable coatings on titanium surfaces. Moreover, the adhesion strength of these coatings can be further improved by chemical and thermal pre-treatment of titanium surfaces as revealed by nano-scratch tests.

Our findings indicate that applying these coatings onto titanium surfaces can significantly improve their biocompatibility, increasing cell adhesion and viability.

CRediT authorship contribution statement

Amir Elhadad: Formal analysis, Methodology, Writing – original draft, Writing – review & editing. **Mohamed A. Mezour:** Data curation, Methodology. **Lina Abu Nada:** Data curation, Investigation. **Samar Shurbaji:** Methodology. **Alaa Mansour:** Formal analysis. **Sophia Smith:** Methodology. **Hanan Moussa:** Writing – review & editing. **Lisa lee:** Data curation. **Eva M. Pérez-Soriano:** Software, Writing – review & editing. **Monzur Murshed:** Supervision, Writing – review & editing. **Richard Chromik:** Supervision. **Faleh Tamimi:** Funding acquisition, Project administration, Writing – review & editing.

Declaration of competing interest

The authors declare that they have no known competing financial interests or personal relationships that could have appeared to influence the work reported in this paper.

Data availability

The data that has been used is confidential.

Acknowledgment

The authors would like to acknowledge Le Réseau de recherche en santé buccodentaire et osseuse (RSBO), Canada Research Chairs (CRC), the Natural Sciences and Engineering Research Council of Canada (NSERC) for their financial support, Qatar University, and the Libyan ministry of education and scientific research.

References

[1] E.J. Delgado-Pujol, et al., Porous beta titanium alloy coated with a therapeutic biopolymeric composite to improve tribomechanical and biofunctional balance, Mater. Chem. Phys. 300 (2023) 127559.
[2] B. Wang, et al., Porous surface with fusion peptides embedded in strontium titanate nanotubes elevates osteogenic and antibacterial activity of additively manufactured titanium alloy, Colloids Surf. B Biointerfaces 224 (2023) 113188.
[3] F. García-Galván, et al., Organic-inorganic hybrid coatings containing phosphorus precursors prepared by sol–gel on Ti6Al4V alloy: electrochemical and in-vitro biocompatibility evaluation, Prog. Org. Coating 148 (2020) 105834.
[4] J. Stepanovska, et al., Treatments for enhancing the biocompatibility of titanium implants, Biomedical Papers of the Medical Faculty of Palacky University in Olomouc 164 (1) (2020).
[5] A. Civantos, et al., Titanium coatings and surface modifications: toward clinically useful bioactive implants, ACS Biomater. Sci. Eng. 3 (7) (2017) 1245–1261.
[6] A. Abdal-hay, et al., Magnesium-particle/polyurethane composite layer coating on titanium surfaces for orthopedic applications, Eur. Polym. J. 112 (2019) 555–568.
[7] V. Barranco, et al., Triethylphosphite as a network forming agent enhances in vitro biocompatibility and corrosion protection of hybrid organic–inorganic sol–gel coatings for Ti6Al4V alloys, J. Mater. Chem. B 2 (45) (2014) 7955–7963.
[8] A.A. El Hadad, et al., Biocompatibility and corrosion protection behaviour of hydroxyapatite sol-gel-derived coatings on Ti6Al4V alloy, Materials 10 (2) (2017) 94.
[9] F. Visentin, et al., TiO2-HA bi-layer coatings for improving the bioactivity and service-life of Ti dental implants, Surf. Coating. Technol. 378 (2019) 125049.
[10] I.A. Neacsu, et al., Biomimetic Collagen/Zn2+-Substituted calcium phosphate composite coatings on titanium substrates as prospective bioactive layer for implants: a comparative study spin coating vs. MAPLE, Nanomaterials 9 (5) (2019) 692.
[11] H. Zhou, et al., Magnesium-based biomaterials as emerging agents for bone repair and regeneration: from mechanism to application, J. Magnesium Alloys 9 (3) (2021) 779–804.
[12] A. Abdal-hay, et al., Novel polycaprolactone/hydroxyapatite nanocomposite fibrous scaffolds by direct melt-electrospinning writing, Eur. Polym. J. 105 (2018) 257–264.
[13] A. Abdal-Hay, et al., Biosynthesis of bonelike apatite 2D nanoplate structures using fenugreek seed extract, Nanomaterials 10 (5) (2020) 919.
[14] J.-z. Lin, et al., Lithium-modified MAO coating enhances corrosion resistance and osteogenic differentiation for pure magnesium, Surface. Interfac. 22 (2021) 100805.
[15] F. Schönweger, et al., New insights into osteointegration and delamination from a multidisciplinary investigation of a failed hydroxyapatite-coated hip joint replacement, Materials 13 (21) (2020) 4713.
[16] N. Ignjatović, et al., Interdisciplinary crossover for rapid advancements-collaboration between medical and engineering scientists with the focus on Serbia, Srp. Arh. Celok. Lek. 149 (3–4) (2021) 229–235.
[17] A.K. Gupta, et al., Evaluation of biphasic hydroxapatite and β-tricalcium phosphate as a bone graft material in the treatment of periodontal vertical bony defects–A clinical and digital radiological measurement study, Indian J. Dent. Res. 33 (2) (2022) 152–157.
[18] X. Lu, et al., A systematic review and network meta-analysis of biomedical Mg alloy and surface coatings in orthopedic application, in: Bioinorganic Chemistry and Applications, 2022, 2022.
[19] W. Jahnen-Dechent, M. Ketteler, Magnesium basics, Clinical kidney journal 5 (Suppl_1) (2012) i3–i14.
[20] D. Fiorentini, et al., Magnesium: biochemistry, nutrition, detection, and social impact of diseases linked to its deficiency, Nutrients 13 (4) (2021) 1136.
[21] M.N.M. Hamad, Magnesium Switch Key of COVID. 19 Morbidity, Mortality and Treatment, 2021.
[22] E. Ray, et al., Physiology of a forgotten electrolyte—magnesium disorders, Advances in Kidney Disease and Health 30 (2) (2023) 148–163.
[23] Y. Ding, et al., Effects of alloying elements on the corrosion behavior and biocompatibility of biodegradable magnesium alloys: a review, J. Mater. Chem. B 2 (14) (2014) 1912–1933.
[24] Y. Leng, A. Soares, Understanding the mechanisms of biological struvite biomineralisation, Chemosphere 281 (2021) 130986.
[25] X. Gu, et al., Biodegradable magnesium phosphates in biomedical applications, J. Mater. Chem. B 10 (13) (2022) 2097–2112.
[26] M. Laurenti, et al., Two-dimensional magnesium phosphate nanosheets form highly thixotropic gels that up-regulate bone formation, Nano Lett. 16 (8) (2016) 4779–4787.
[27] T. Albrektsson, A. Wennerberg, On osseointegration in relation to implant surfaces, Clin. Implant Dent. Relat. Res. 21 (2019) 4–7.
[28] P.S. Kumar, et al., The effects of titanium implant surface topography on osseointegration: literature review, JMIR Biomedical Engineering 4 (1) (2019) e13237.
[29] F.R. García-Galván, et al., Sol-gel TiO2 and ZrO2-nanocomposite thin films for enhancing in vitro biocompatibility and bio-corrosion resistance of Ti6Al4V orthopaedic implants, in: Electrochemical Society Meeting Abstracts, vol. 230, The Electrochemical Society, Inc, 2016.
[30] V. Jandová, et al., Corrosion behavior of titanium silicide surface with hydrogen peroxide: formation of sub-μm TiOx-based spheres, nanocomposite TiOx/SiOx phases, and mesoporous TiOx/SiOx network, Appl. Surf. Sci. 529 (2020) 147133.
[31] E. Peón Avés, et al., Comparative study of hydroxyapatite coatings obtained by Sol-Gel and electrophoresis on titanium sheets, Materia 12 (2007) 156–163.
[32] A. Mansour, et al., Bone extracts immunomodulate and enhance the regenerative performance of dicalcium phosphates bioceramics, Acta Biomater. 89 (2019) 343–358.
[33] D. Velten, et al., Characterization of thermal and anodic oxide layers on β-and on near-β-titanium alloys for biomedical application, Int. J. Mater. Res. 94 (6) (2022) 667–675.
[34] T.M. Salama, et al., Titanate Nanotubes Coated with Ag Nanoparticles: Effects of Annealing Temperature on Crystalline Structure, Morphology, and Photocatalytic Activity, 2024.
[35] A.V. Ponaryadov, et al., Natural titanium dioxide nanotubes, Epitoanyag-Journal of Silicate Based & Composite Materials 72 (5) (2020).
[36] S.-W. Choi, et al., Grade-4 commercially pure titanium with ultrahigh strength achieved by twinning-induced grain refinement through cryogenic deformation, J. Mater. Sci. Technol. 66 (2021) 193–201.
[37] M. Chandrika, et al., Potato starch assisted sodium hydrogen titanium oxide/titanium dioxide nanostructures and annealing effects, Appl. Phys. A 128 (2) (2022) 163.
[38] Z. Noer, et al., Effects of the calcination atmosphere and pre-heating treatment on the characteristics of sodium titanate nanorods synthesized from titanium tetraisopropoxide-sodium chloride precursors assisted by organic templates, J. Ceram. Soc. Jpn. 128 (7) (2020) 415–423.
[39] T. Kizuki, et al., Effect of Ca contamination on apatite formation in a Ti metal subjected to NaOH and heat treatments, J. Mater. Sci. Mater. Med. 24 (3) (2013) 635–644.
[40] A.A. Al-Hashedi, et al., Decontamination of titanium implants using physical methods, Clin. Oral Implants Res. 28 (8) (2017) 1013–1021.
[41] L. Liv, Z. Demirel, Ponceau polymer film for electrocatalytic sensing of levodopa in human serum, urine, and pharmaceutical formulation, Microchem. J. 197 (2024) 109784.
[42] C. Sheng, et al., One-step hydrothermal method to prepare superhydrophobic cotton fabric with antibacterial properties, Journal of Engineered Fibers and Fabrics 16 (2021) 15589250211066095.
[43] S. Dey, et al., Probing Defect Induced Room Temperature Ferromagnetism in CVD Grown MoO3 Flakes: A Correlation with Electronic Structure and First Principle-Based Calculations, 2023 arXiv preprint arXiv:2309.02277.
[44] M. Murphy, et al., Toward optimizing dental implant performance: surface characterization of Ti and TiZr implant materials, Dent. Mater. 33 (1) (2017) 43–53.
[45] D.-Y. Lin, X.-X. Wang, Preparation of hydroxyapatite coating on smooth implant surface by electrodeposition, Ceram. Int. 37 (1) (2011) 403–406.
[46] Y. Yao, et al., Engineered biochar reclaiming phosphate from aqueous solutions: mechanisms and potential application as a slow-release fertilizer, Environ. Sci. Technol. 47 (15) (2013) 8700–8708.
[47] U. Sulaeman, et al., Data of XPS in incorporating the platinum complexes dopant on the surface of Ag3PO4 photocatalyst, Data Brief 28 (2020) 104988.
[48] S. Galli, et al., Local release of magnesium from mesoporous TiO2 coatings stimulates the peri-implant expression of osteogenic markers and improves osteoconductivity in vivo, Acta Biomater. 10 (12) (2014) 5193–5201.
[49] P. Xie, et al., Analysis and prediction of the gas-liquid interfacial area for droplets impact on solid surfaces, Appl. Therm. Eng. 178 (2020) 115583.
[50] L.M. Pandey, S.K. Pattanayek, Hybrid surface from self-assembled layer and its effect on protein adsorption, Appl. Surf. Sci. 257 (10) (2011) 4731–4737.
[51] F. Jia, et al., Strontium-calcium doped titanium dioxide nanotubes loaded with GL13K for promotion of antibacterial activity, anti-Inflammation, and vascularized bone regeneration, Ceram. Int. 49 (22) (2023) 35703–35721.
[52] C.-T. Hsiao, et al., Fibronectin in cell adhesion and migration via N-glycosylation, Oncotarget 8 (41) (2017) 70653.

[53] E.-J. Lee, et al., Identification of novel FNIN2 and FNIN3 fibronectin-derived peptides that promote cell adhesion, proliferation and differentiation in primary cells and stem cells, Int. J. Mol. Sci. 22 (6) (2021) 3042.
[54] C.J. Dalton, C.A. Lemmon, Fibronectin: molecular structure, fibrillar structure and mechanochemical signaling, Cells 10 (9) (2021) 2443.
[55] Y. Luo, et al., Surface treatment functionalization of sodium hydroxide onto 3D printed porous Ti6Al4V for improved biological activities and osteogenic potencies, J. Mater. Res. Technol. 9 (6) (2020) 13661–13670.
[56] M.P. Staiger, et al., Magnesium and its alloys as orthopedic biomaterials: a review, Biomaterials 27 (9) (2006) 1728–1734.
[57] X. Nie, et al., Effect of magnesium ions/Type I collagen promote the biological behavior of osteoblasts and its mechanism, Regenerative Biomaterials 7 (1) (2020) 53–61.
[58] R.K. Rude, et al., Skeletal and hormonal effects of magnesium deficiency, J. Am. Coll. Nutr. 28 (2) (2009) 131–141.